How oxygen attacks [FeFe] hydrogenases from photosynthetic organisms

Sven T. Stripp[a], Gabrielle Goldet[b], Caterina Brandmayr[b], Oliver Sanganas[c], Kylie A. Vincent[b], Michael Haumann[c], Fraser A. Armstrong[b], and Thomas Happe[a,1]

[a]Lehrstuhl Biochemie der Pflanzen, AG Photobiotechnologie, Ruhr Universität Bochum, Universitätsstrasse 150, 44801 Bochum, Germany; [b]Inorganic Chemistry Laboratory, University of Oxford, South Parks Road, Oxford OX1 3QR, United Kingdom; and [c]Institut für Experimentalphysik, Freie Universität Berlin, Arnimallee 14, 14195 Berlin, Germany

Edited by Bob B. Buchanan, University of California, Berkeley, CA, and approved August 28, 2009 (received for review May 14, 2009)

Green algae such as *Chlamydomonas reinhardtii* synthesize an [FeFe] hydrogenase that is highly active in hydrogen evolution. However, the extreme sensitivity of [FeFe] hydrogenases to oxygen presents a major challenge for exploiting these organisms to achieve sustainable photosynthetic hydrogen production. In this study, the mechanism of oxygen inactivation of the [FeFe] hydrogenase *Cr*HydA1 from *C. reinhardtii* has been investigated. X-ray absorption spectroscopy shows that reaction with oxygen results in destruction of the [4Fe-4S] domain of the active site H-cluster while leaving the di-iron domain ($2Fe_H$) essentially intact. By protein film electrochemistry we were able to determine the order of events leading up to this destruction. Carbon monoxide, a competitive inhibitor of *Cr*HydA1 which binds to an Fe atom of the $2Fe_H$ domain and is otherwise not known to attack FeS clusters in proteins, reacts nearly two orders of magnitude faster than oxygen and protects the enzyme against oxygen damage. These results therefore show that destruction of the [4Fe-4S] cluster is initiated by binding and reduction of oxygen at the di-iron domain—a key step that is blocked by carbon monoxide. The relatively slow attack by oxygen compared to carbon monoxide suggests that a very high level of discrimination can be achieved by subtle factors such as electronic effects (specific orbital overlap requirements) and steric constraints at the active site.

EXAFS | H-cluster | protein film electrochemistry | biological hydrogen production | green algae

Hydrogenases are ubiquitous in bacteria and archaea but are also found in some eukaryotes, particularly green algae (1). There are three distinct classes, known as [NiFe]-, [FeFe]-, and [Fe] hydrogenases, based on the metal components of the active site that binds or releases H_2 (2).

Many hydrogenases have extremely high activities (3), a fact that has been emphasized most recently in studies by protein film electrochemistry (4–6). Hydrogenases are able to catalyze both H_2 oxidation and H_2 evolution with minimal electrochemical overpotential (driving force) (4, 7), comparable to the $2H^+/H_2$ equilibrium established on platinum (5). The [FeFe] hydrogenases are of particular interest as they tend to be more biased toward H_2 evolution than [NiFe] hydrogenases (8). The active site of [FeFe] hydrogenases, a complex structure known as the "H-cluster," consists of a binuclear Fe center ($2Fe_H$) linked to a [4Fe-4S] cluster (9). Numerous publications report the chemical synthesis of analogues for the $2Fe_H$ domain and even the entire H-cluster (10)—such is the interest displayed not only in understanding the enzymes, but also in finding cheap alternatives to Pt catalysts. However, [FeFe] hydrogenases are extremely prone to irreversible inactivation by O_2, and this sensitivity is a key challenge for both the biotechnological and the synthetic chemistry approaches (8).

Viewed in detail, the $2Fe_H$ domain consists of iron atoms Fe_p and Fe_d that are, respectively, proximal and distal relative to the [4Fe-4S] domain that is connected to Fe_p by a bridging cysteine sulfur (9). An unusual dithiolate ligand, originally modeled as a 1,3 propane dithiolate, forms a bridge between Fe_p and Fe_d. In the oxidized state H_{ox}, as determined from the structure of the *Cp*I enzyme from *Clostridium pasteurianum*, Fe_p is also coordinated by one CO and one CN^- ligand and shares a bridging CO with Fe_d (11, 12). The distal Fe is also coordinated by one CO and one CN^- ligand, and an additional binding site is vacant (9) or occupied by an exchangeable O ligand, most likely a water molecule (11). In the structure of the [FeFe] hydrogenase from *Desulfovibrio desulfuricans*, which is believed to be crystallized in the H_{red} form, the bridging CO is replaced by a terminal CO on Fe_d (13). A recent EPR analysis favors an oxidation state assignment of $[4Fe\text{-}4S]^{2+}\text{-}Fe_p(I)Fe_d(II)$ for H_{ox}, with some spin density delocalized onto the [4Fe-4S] domain (14). The EPR-silent H_{red} state is assigned as $[4Fe\text{-}4S]^{2+}\text{-}Fe_p(I)Fe_d(I)$ or a hydrido species $[4Fe\text{-}4S]^{2+}\text{-}Fe_p(II)Fe_d(II)\text{-}H^-$, and it appears that the [4Fe-4S] cluster may not access the 1+ level in anything other than a transient manner (15). Crystallography and infrared spectroscopy has shown that exogenous CO, a competitive inhibitor, attacks $2Fe_H$ at the vacant/exchangeable binding site of Fe_d (16–18). Carbon monoxide is a π-acceptor ligand and binds to electron-rich transition metals (19). From a molecular orbital perspective, H_2 resembles CO because, by analogy with the Dewar-Chatt-Duncanson model for binding of alkenes to metals (20), back donation of electron density into the antibonding σ-orbital of molecular H_2 is important for its binding and activation (20). These facts are highly relevant because they form the basis for CO being competitive with H_2 (21) during H_2 oxidation, and therefore, Fe_d is likely to be the site for H_2 binding (17). Like CO, O_2 is also a π-acceptor ligand and likely to bind to the same site(s); we can anticipate that any such binding could result in the generation of highly reactive oxygen intermediates (22, 23).

Here, we present a study of the mechanism by which O_2 irreversibly attacks the H-cluster, by using electrochemical kinetics with the *reversible* inhibitor CO as a complementary probe. By using X-ray absorption spectroscopy (XAS) at the Fe K-edge, we examine, at atomic level resolution, the nature of the product obtained. Our subject is the [FeFe] hydrogenase *Cr*HydA1 from the photosynthetic green alga *Chlamydomonas reinhardtii*. The [FeFe] hydrogenases of green algae are of particular interest for photosynthetic H_2 production (8) and because this class of hydrogenase enzymes contain *only* the H-cluster (24–26) it is possible to interpret the XAS data without interference from additional electron-transferring FeS clusters that are present in bacterial hydrogenases (9, 11). The results

Author contributions: S.T.S., G.G., K.A.V., M.H., F.A.A., and T.H. designed research; S.T.S., G.G., C.B., O.S., and M.H. performed research; S.T.S., G.G., C.B., O.S., K.A.V., M.H., F.A.A., and T.H. analyzed data; and S.T.S., G.G., M.H., F.A.A., and T.H. wrote the paper.

The authors declare no conflict of interest.

This article is a PNAS Direct Submission.

[1]To whom correspondence should be addressed. E-mail: thomas.happe@rub.de.

This article contains supporting information online at www.pnas.org/cgi/content/full/0905343106/DCSupplemental.

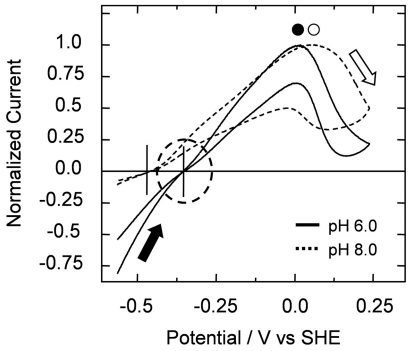

Fig. 1. Catalytic profile of *Cr*HydA1 at pH 6.0 (solid lines) and pH 8.0 (dashed lines) as viewed by cyclic voltammograms of the enzyme adsorbed on a PGE electrode. The thermodynamic $2H^+/H_2$ potentials at pH 6.0 and pH 8.0 are marked by the vertical lines. The dashed oval highlights the inflection point at the zero-current potential at pH 6.0. Black and open circles mark the potential at which anaerobic inactivation begins to occur as the potential is swept to more positive values and the current at each cyclic voltammogram has been normalized at this potential. Black and open arrows indicate the directions of the scans at pH 6 and pH 8, respectively. Experimental conditions: 20 °C, 1 bar H_2, electrode rotation rate 3,000 rpm, scan rate 20 mV/s.

lead to a mechanistic model of how [FeFe] hydrogenases are inactivated by O_2.

Results

Protein Film Electrochemistry. Cyclic voltammograms recorded for *C. reinhardtii* [FeFe] hydrogenase *Cr*HydA1 at 1 bar H_2 show the relative activities for H^+ reduction and H_2 oxidation (Fig. 1). The graph displays two distinct scans obtained at pH 6.0 and pH 8.0 at 20 °C. The potential is swept from −0.55 V to + 0.24 V vs. SHE and then scanned back to −0.55 V. The enzyme is clearly a bidirectional hydrogenase; at pH 6.0 (solid line), the catalytic activities for H^+ reduction compared to H_2 oxidation are approximately comparable, whereas at pH 8.0 (dashed line), the activity for H^+ reduction is much lower, most obviously because the H^+ concentration is two orders of magnitude lower. In either case the voltammograms cut through the zero-current line (potential axis) at the potential expected for the $2H^+/H_2$ redox couple under these conditions. The slight inflection detectable in this region (dashed oval in Fig. 1) suggests that a small overpotential is required for efficient electron transport to and from the active site. At high potentials (> 0 V vs. SHE, see circles) the enzyme inactivates, giving rise to the anaerobically oxidized state [H_{ox}inact (7)]. This is apparent from the decrease in H_2 oxidation current, which recovers at least partially on the return scan. The reversibility of this inactivation depends on pH, and it is much more reversible at pH 6.

The kinetics of O_2 inactivation of H_2 oxidation were investigated by chronoamperometric experiments in which the current was monitored following changes in gas composition. The catalytic current is a direct measure of enzymatic turnover rate. Fig. 2 shows the dependence of inactivation rate on O_2 level (Fig. 2*A*) and H_2 level (Fig. 2*B*). In all experiments the cell potential was set to −0.05 V vs. SHE to optimize the H_2 oxidation rate while avoiding anaerobic inactivation (see circles in Fig. 1). Experiments were performed at pH 6.0, 20 °C. Reactions with O_2 were initiated by changing the gas composition flowing in the headspace of the cell and simultaneously injecting a solution of buffer preequilibrated with the desired gas composition. This combination of operations ensured rapid initiation and a constant O_2 level throughout the reaction. An important feature of these experiments was that the H_2 concentration in solution always remained constant. Control experiments were performed to assess the current contribution because of direct reduction of O_2 at the graphite electrode, although this was small at −0.05 V (see *SI Text* and Fig. S1). In all cases O_2 caused almost complete inactivation (>95%).

Fig. 2*A* shows how the rate of inactivation depends on the concentration of O_2 (0.5%, 5%, and 10%) with 80% H_2 as the carrier gas and N_2 making up the remaining fraction. Each experiment commenced with 80% H_2 and 20% N_2 flushing through the cell, then O_2 was introduced, as explained above, and once the enzyme was fully inactivated, the original headgas composition was restored by changing the incoming gas mixture back to 80% H_2 and 20% N_2. The time-courses conformed to first-order exponential behavior for one to two half lives and rates were also first order in O_2 up to at least 15% O_2 headgas

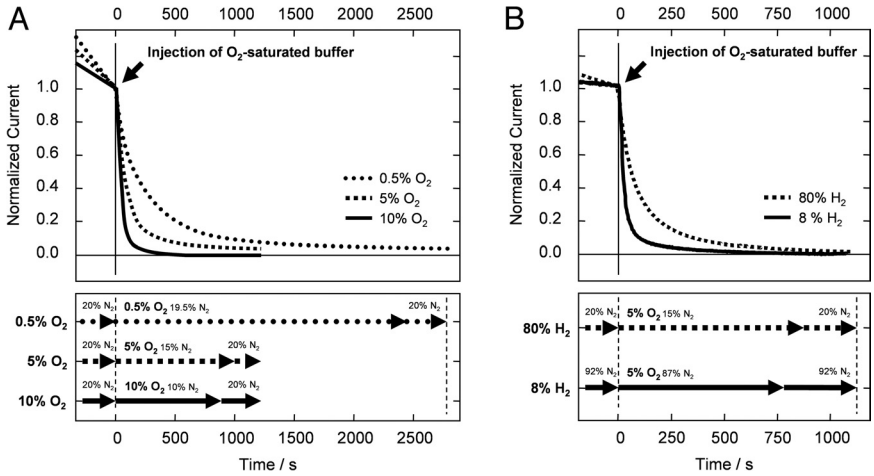

Fig. 2. Inactivation of *Cr*HydA1 by O_2 by simultaneous gas exchange and injection of O_2-saturated buffers. Experiments were carried out under (*A*) different concentrations of O_2 and (*B*) different concentrations of H_2. (*A*) Gas mixtures in the headspace contain 80% H_2 and the remaining 20% are as indicated. For the experiments in which inactivation was induced by 10% and 5% O_2, injections of 2 mL and 0.67 mL buffer saturated with 20% O_2 and 80% H_2 (respectively) were performed into the cell containing 2 mL at the beginning of the experiment. For the experiments in which inactivation was induced by 0.5% O_2, an injection of 0.5 mL buffer saturated with 2.5% O_2 and 80% H_2 was performed into the cell containing 2 mL at the beginning of the experiment. (*B*) Inactivation was achieved with 5% O_2 in the headspace and the solid and dashed lines represent experiments performed with 8% and 80% H_2, respectively. For the experiments in which inactivation was induced by 5% O_2 in 8% H_2, an injection of 0.67 mL buffer saturated with 20% O_2 and 8% H_2 was performed into the cell initially containing 2 mL. Other conditions: pH 6.0, 20 °C, electrode rotation rate 3,000 rpm, −0.05 V vs. SHE.

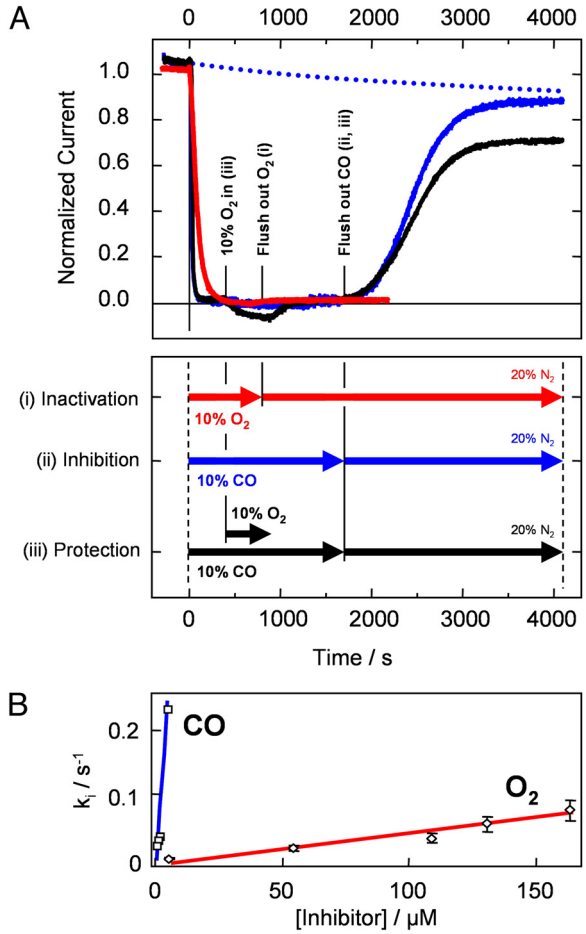

Fig. 3. Inactivation of *Cr*HydA1 by O_2 as compared to inhibition by CO, and protection by CO against O_2 inactivation. (*A*) Inactivation and inhibition by 10% O_2 (i, red trace) and 10% CO (ii, blue trace) by gas exchange. The black trace shows an experiment in which the enzyme was subjected to 10% O_2 after being fully inhibited by 10% CO (iii). The dotted line gives a visual guide to the progression of background film loss. Experimental conditions: pH 6.0, 20 °C, electrode rotation rate 3,000 rpm, −0.05 V vs. SHE, gas mixtures in the headspace as indicated, with 80% H_2 and balance of N_2 making up the remainder of the headspace atmosphere. The timeline shown in the lower panel provides a guide for the sequence of gas changes. (*B*) Dependence of rate of inactivation on concentration of O_2 (diamonds, red) and CO (squares, blue). Note the rates of inactivation by CO were calculated by performing experiments such as those shown in Fig. 2, that is, by simultaneous injection of CO-saturated buffer and gas exchange.

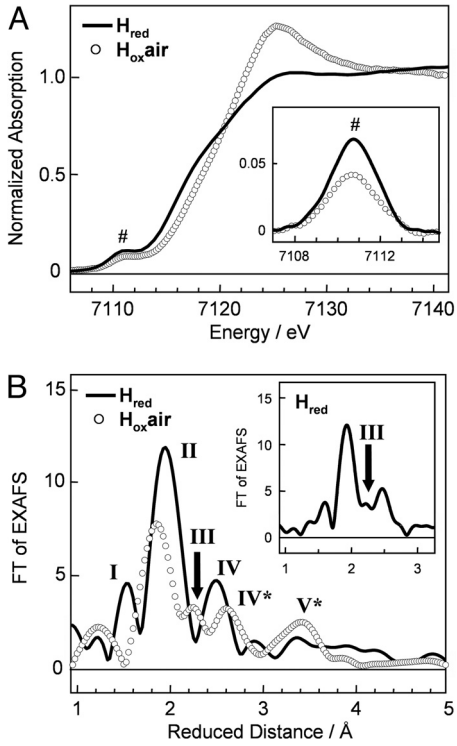

Fig. 4. XAS comparison of *Cr*HydA1 in its as-isolated reduced form (H_{red}) and after O_2 incubation (H_{ox}air). The *reduced* distance is the true metal-backscatterer distance minus approximately 0.4 Å because of a phase shift. (*A*) Fe K-edge spectra. Inset: isolated preedge features due to $1s \rightarrow 3d$ electronic transitions. The shown preedge features were derived by subtraction of a polynomial spline from the main edge rise by using the program Xanda. (*B*) FTs of EXAFS spectra (see Fig. S2) of H_{red} (solid line) and H_{ox}air (open circles). The FTs were calculated for *k* values of 1.6–16.5 $Å^{-1}$ (7.4–19.5 $Å^{-1}$ in the inset). Numbers on the FT peaks denote specific Fe-ligand interactions as discussed in the text. The Fe-Fe distance of $2Fe_H$ of 2.52 Å (FT peak III) is discernable under both conditions; the Fe-Fe distances of approximately 2.7 Å (FT peak IV) from the [4Fe-4S] cluster are largely diminished in H_{red}.

composition (≈0.2 mM in solution) as displayed in Fig. 3*B* (see below). Fig. 2*B* shows that the rate of inactivation of H_2 oxidation by O_2 depends on the H_2 concentration (80% H_2 compared to 8% H_2).

Fig. 3 shows experiments in which CO, known to be a competitive inhibitor of H_2 oxidation (21), is used to probe the course of O_2 attack. Fig. 3*A* shows three experiments performed at pH 6.0, 20 °C, and −0.05 V vs. SHE. The timeline shown in the lower panel of Fig. 3*A* provides a guide for the sequence of gas changes. Hydrogen was maintained at 80% fractional composition in the gas stream throughout all experiments. In the first experiment (*i*), the enzyme is inactivated by introducing 10% O_2 (red trace), and in the second (*ii*), it is inhibited by introducing 10% CO (blue trace). In the third experiment (*iii*), 10% O_2 is introduced to enzyme that is already inhibited by 10% CO (black trace).

The decrease in current because of inhibition by CO (*ii*) is much more rapid than it is for O_2 (*i*), and the comparative rates of inhibition at different inhibitor concentrations are shown in Fig. 3*B*. For comparison the second-order rate constants for inhibition by CO and inactivation by O_2 (obtained from the slopes of the lines in Fig. 3*B*) are 50 $mM^{-1}s^{-1}$ (46 $bar^{-1}s^{-1}$) and 0.43 $mM^{-1}s^{-1}$ (0.47 $bar^{-1}s^{-1}$), respectively. Also, it is clear from Fig. 3*A* that, when the CO is removed from the gas stream, the current increases to a level consistent with that expected based on natural protein film loss from the electrode measured in control experiments over the same period, showing that CO inhibition of H_2 oxidation is reversible. However, removal of O_2 from the cell only results in a tiny increase in current, that is, O_2 inactivation is almost (but not entirely) irreversible. Experiment (*iii*) in Fig. 3*A* demonstrates that CO protects the enzyme against inactivation by O_2 as 80% of the initial activity is recovered on removal of CO from the gas stream. This result agrees with the observation reported recently for another [FeFe] hydrogenase *Ca*HydA from *Clostridium acetobutylicum* (27).

X-Ray Absorption Measurements. Fig. 4 depicts XAS spectra of the as-isolated reduced form of *Cr*HydA1 (H_{red}) and the as-isolated protein after incubation with O_2 (H_{ox}air). The shape of the Fe K-edge spectrum of H_{red} (Fig. 4*A*) reveals a predominant coordination of the Fe atoms by the S atoms of the conserved cysteine residues in *Cr*HydA1 (25); indications for O-ligation to Fe are absent (28, 29). The increased primary K-edge maximum

BIOCHEMISTRY

Table 1. EXAFS fit results

Sample	Shell	Peak	N_i [per Fe atom]	R_i [Å]	$2\sigma^2_i$ [Å^2]	R_F [%]
H_{red}	C(=O/N)	I	0.46	1.76	0.002*	8.7
	S	II	3.57	2.28	0.010*	
	Fe $2Fe_H$	III	0.81	2.52	0.002*	
	Fe [4Fe-4S]	IV	2.06	2.71	0.010*	
H_{ox}air	C(=O/N) / O	I	1.11	1.89	0.002*	11.0
	S	II	2.09	2.26	0.010*	
	Fe $2Fe_H$	III	0.67	2.56	0.002*	
	Fe [4Fe-4S]	IV	0.97	2.77	0.010*	

R_F (39) was calculated over reduced distances of 1.3–2.8 Å. Both simulations comprise a further multiple-scattering Fe(-C)=O/N shell (with the same *N*-value as for the Fe-C(=O/N) shell; average respective distances of 2.98 Å; $2s^2$ was set to 0.01 Å^2). N_i, coordination number; R_i, Fe-ligand distance; $2s^2_i$, Debye-Waller factor.
*Fixed values in the fit procedure.

at approximately 7,125 eV and a decreased preedge amplitude (# at ~7,111 eV, inset) in H_{ox}air clearly suggest the binding of O-atom ligands to Fe ions that subsequently became more symmetrically coordinated (25). This result may be explained by binding of additional O-species to the H-cluster and partial release of Fe from the protein in the form of hexaquo-Fe(II) ions.

Fourier transforms (FTs) of EXAFS spectra for H_{red} and H_{ox}air are shown in Fig. 4*B*. The FT of the H_{red} spectrum (solid line and inset) shows four main peaks I - IV. The reduced distances given in the figure are approximately 0.4 Å smaller than the true metal-ligand distances because of a phase shift. These peaks reflect different Fe interactions of the H-cluster, namely Fe-C(= O/N) (I), Fe-S (II), and Fe-Fe (IV) (25). An additional peak III became visible in H_{red} when the FT was calculated from the corresponding EXAFS oscillations starting at higher *k*-values and extending over a longer *k*-range (inset, see Fig. S2). This feature represents the Fe-Fe interaction in the $2Fe_H$ moiety (25). Peak III in the spectrum of H_{ox}air is also attributable to this Fe-Fe interaction. Diminished Fe-Fe interactions from the cubane cluster in the H_{ox}air spectrum allow for discrimination of peak III even in FT spectra calculated from a *k*-range starting at lower values. Contributions to the EXAFS spectra from multiple-scattering (MS) effects of the near-linear Fe-C = O/N arrangements are small (25) because of their relatively low coordination number and interference with the Fe-Fe interactions of the [4Fe-4S] cluster.

Precise Fe-ligand distances were determined by simulations of the EXAFS spectra. The coordination numbers per Fe ion (N_i) and the Fe-ligand and Fe-Fe distances (R_i) for H_{red} (Table 1) are compatible with the expected structure of the reduced H-cluster H_{red} in *Cr*HydA1. Whereas H_{ox} is reported to be in the Fe_p(I)-Fe_d(II) state and has a 'bridging' CO between Fe_p and Fe_d, H_{red} is assigned as Fe_p(I)-Fe_d(I) and lacks the bridging CO that has become a terminal ligand to Fe_d (14, 17, 24, 25). In particular, the Fe-Fe distances of 2.52 Å for the $2Fe_H$ moiety (III, inset in Fig. 4*B*) and 2.71 Å for the [4Fe-4S] moiety (IV) can clearly be distinguished by EXAFS.

The FT of the EXAFS spectrum of the O_2-treated enzyme (H_{ox}air in Fig. 4*B*, open circles) reveals a missing contribution from Fe-Fe interactions of the [4Fe-4S] cluster (IV in H_{red}). In addition, a shift of the main FT peak (II) to shorter distances is observed. This is because of contributions from Fe-O bonds, which are shorter than Fe-S bonds. Peak I (representing Fe-C(= O/N) interactions in H_{red}) appears decreased in size in H_{ox}air. This is attributable to interference between Fe-O and Fe-C(= O/N) contributions that cannot easily be discriminated. For H_{ox}air the $2Fe_H$-specific FT feature III is even more distinct than in H_{red} (inset). Peaks exclusively appearing in the H_{ox}air spectrum are marked with asterisks. Peak IV*, which is indicative of MS contributions from the C = (O/N) ligands is resolved more clearly because peak IV is essentially diminished in H_{ox}air. That the Fe atoms of the [4Fe-4S] cluster may remain bound to the protein but coordinate additional O-ligands is suggested by the observed FT peak V*, which may correspond to long Fe-O-Fe binding motifs (28) prominent in H_{ox}air only.

Simulations of the H_{ox}air EXAFS spectrum (Table 1) revealed that in H_{ox}air the Fe-Fe distance in $2Fe_H$ is 0.04 Å longer than the Fe-Fe distance in H_{red} (2.56 and 2.52 Å, respectively), with a coordination number lowered by only ≈20%. This is compatible with a Fe-Fe distance elongation upon oxidation from H_{red} to H_{ox}-CO which we reported recently (25). Accordingly, a fraction of approximately 80% of protein may be calculated to retain a normal $2Fe_H$ unit in which the overall structure is preserved upon O_2 treatment. Distance elongation may be caused by binding of O-species to $2Fe_H$. In contrast, there was a 2-fold decrease of the approximately 2.7 Å Fe-Fe interactions (from N_i 2.06 to 0.97 in H_{ox}air) per Fe ion, because of the loss of respective motifs in the [4Fe-4S] cluster. Therefore, in more than half of the protein molecules the native structure of the [4Fe-4S] cluster is degraded.

In summary, the XAS results show that exposure of *Cr*HydA1 to O_2 causes modification or destruction of the [4Fe-4S] domain of the H-cluster, with the coordination shell of the $2Fe_H$ domain remaining relatively unchanged.

Discussion

The electrocatalytic response of *Cr*HydA1 shows that the enzyme exhibits very similar characteristics to other hydrogenases (30). In electrochemical experiments, the enzyme's activity is directly measured through the catalytic current. The inflection point at the zero-current potential observed for *Cr*HydA1 contrasts with the sharp intersection with the zero-current axis exhibited by other (bacterial) hydrogenases (6, 7, 27). This may be because of the absence of an electron-transfer relay in *Cr*HydA1 (26) and reflects a small overpotential requirement to drive electrons in either direction. Catalytically, the enzyme is bidirectional and its proficiency in H_2 oxidation allows us to measure *directly* the competition between H_2, CO, and O_2. Note that continuous recording of the time course of H_2 evolution, which requires a low potential or strong reductant, are complicated in the presence of O_2.

Several observations point to a mechanism in which damage by O_2 requires its prior attack at the $2Fe_H$ domain. First, exogenous CO, known to bind at the distal Fe site (17) and be a competitive inhibitor of H_2 oxidation (21), protects the enzyme against inactivation by O_2. Second, the rate of inactivation by O_2 is lower at high H_2 levels, in line with the competitive relationship between CO and H_2. Third, there are many examples of O_2 and its partial reduction products known as 'reactive oxygen species' (ROS) attacking FeS clusters, including fumarate-nitrate regulatory protein (FNR) (22). Fourth, there is *no* precedent for CO directly attacking [4Fe-4S] clusters in proteins.

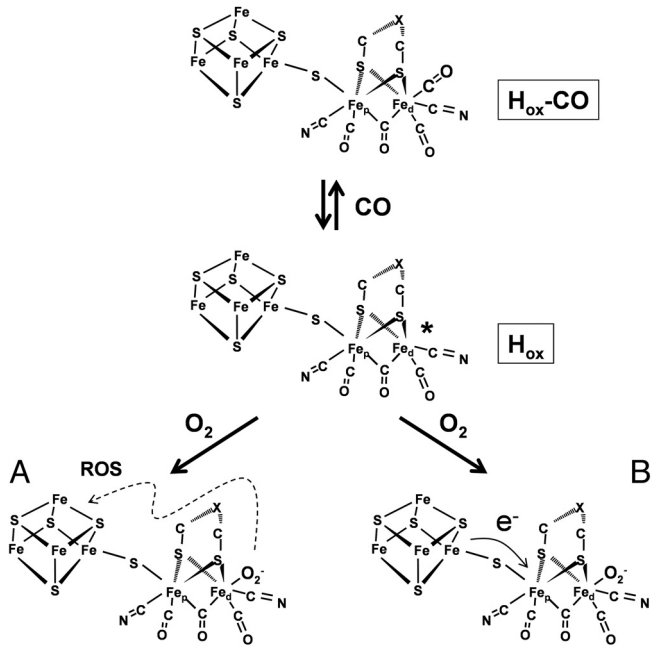

Fig. 5. Model scheme for reaction of CO and O_2 with the H-cluster. Carbon monoxide binds reversibly to the oxidized state H_{ox}, giving an inhibited species H_{ox}-CO. Oxygen reacts by binding to the H-cluster at the same site as CO, that is, Fe_d. The O_2 is converted to a reactive oxygen species (ROS), most likely superoxide (formed by one electron reduction). The ROS can either migrate the very short distance to oxidize the $[4Fe\text{-}4S]^{2+}$ cluster (*A*) or it can remain bound and exert its destructive effect by causing a through-bond electron transfer from the [4Fe-4S] cluster (*B*).

The observation from EXAFS, that the fate of the H-cluster in its reaction with O_2 is a modification of the [4Fe-4S] domain rather than of the $2Fe_H$ domain, in conjunction with the protective effect of CO, together mean that the reaction of O_2 with the $2Fe_H$ domain (as argued above) generates a species that subsequently attacks the [4Fe-4S] domain. In Fig. 5, we consider two mechanisms by which this could occur. The first option involves O_2 reacting at the $2Fe_H$ domain to form a ROS, particularly superoxide, that migrates the short distance to attack the [4Fe-4S] cluster. The second option involves superoxide being formed by reaction with the $2Fe_H$ domain but remaining bound (presumably at the distal Fe site) as a strong oxidant, inflicting long-range oxidation of the [4Fe-4S]-cluster by through-bond electron transfer. Direct attack of O_2 on the [4Fe-4S] cluster might be prevented by steric effects, or be less favorable, thermodynamically, because superoxide (0.9 V) is a much stronger one-electron oxidant than O_2 (< -0.1 V). In either of these two mechanisms, it is likely that O_2 attacks the H-cluster in the oxidation level H_{ox} that is assigned as $[4Fe\text{-}4S]^{2+}$-$Fe_p(I)Fe_d(II)$. This proposal is based on analogy with observations made with CO, which is known to bind preferentially to H_{ox} relative to H_{red} (giving a characteristic EPR-detectable form known as H_{ox}-CO) (14, 17) [Under anaerobic conditions, it is widely reported that H_{ox} can be oxidized reversibly to the state H_{ox}inact, correspondingly formulated as $[4Fe\text{-}4S]^{2+}$-$Fe_p(II)Fe_d(II)$ (7, 31)]. It is well-established that [4Fe-4S] clusters are prone to oxidative damage via sequences involving some or all of the following: (*i*) initial formation of superoxidized species such as $[4Fe\text{-}4S]^{3+}$ (*ii*) subsequent ejection of Fe giving a [3Fe-4S] cluster (32–35), (*iii*) further loss of Fe and S, and (*iv*) complete breakdown of the cluster. As an example, oxidative breakdown of a [4Fe-4S] cluster by such a sequence is found for FNR, an O_2 sensing protein (22, 36). Oxidative degradation of [4Fe-4S] clusters in ferredoxins without O_2, that is, by an anaerobic pathway, has been studied by cyclic voltammetry and electrochemical potential pulse experiments (34, 35). These studies showed a correlation between the air-stabilities of [4Fe-4S] clusters in different proteins and the electrode potential required to induce their anaerobic oxidative damage via a [3Fe-4S] intermediate. Our observation that anaerobic inactivation of *Cr*HydA1 is only partially reversible may be relevant to the O_2 mechanism because it suggests the ease by which the [4Fe-4S] domain could be damaged by a long-range electron-transfer process, as would be the case if the ROS did not leave the $2Fe_H$ domain.

The observation that CO reacts so much faster than O_2 leads us to question the effectiveness of a 'gas filter' within the enzyme and to suggest instead that more effective gas discrimination occurs in the highly specific region of the active site. In the close proximity of the H-cluster, electronic and steric influences of the protein environment are likely to determine the efficiency of ligand binding. In the case of *Cr*HydA1, we were able to show that binding of CO is kinetically favored about O_2 and H_2 ligation. There is already a precedent for such discrimination, in the reverse direction, in the case of the [NiFe] uptake hydrogenases from *Ralstonia eutropha* and *R. metallidurans*. For those enzymes, which are highly O_2-tolerant, CO (a strong π-acceptor ligand) is a very weak inhibitor (37): even more significantly, in H_2 evolution, H_2 is a far superior inhibitor to either CO or O_2. These effects must arise from differences in the geometries of coordination imposed by the local environment, and we propose that similar principles could be applied to selectivity at the $2Fe_H$ domain.

Materials and Methods

Recombinant *C. reinhardtii* [FeFe] hydrogenase *Cr*HydA1 was synthesized and isolated anaerobically from *C. acetobutylicum* as previously described (38). To prepare samples for XAS, isolated protein was concentrated to 1 mM (48 g/L) by using Vivaspin 6 and Vivaspin 500 columns (Sartorius Stedim Biotech) and stored in 0.1 mM Tris/HCl pH 8.0, 2 mM sodium dithionite (NaDT), and 10% glycerol. To obtain an O_2-treated sample, the protein sample was dialyzed with NaDT-free 0.1 M Tris/HCl pH 8.0 before concentration. Protein samples (30 μL, 1 mM) were placed in 200 μL PCR tubes (Eppendorf) and loaded into 8 mL glass tubes. The tubes were then sealed with a septum and taken out of the anaerobic glovebox (Coy Laboratories, N_2 atmosphere with approximately 5% H_2 and $O_2 < 2$ ppm). The headgas of the sealed tubes was flushed with moistened O_2 (Air Products, 15 min) and argon (Air Liquide, 5 min) giving the irreversibly damaged form ''H_{ox}air''. During O_2 treatment, the protein was kept on ice. A sample of *Cr*HydA1 as-isolated and reduced by 2 mM NaDT (26) is referred to as ''H_{red}''. Samples of H_{ox}air and H_{red} were transferred to Kapton-covered acrylic-glass XAS sample holders and then rapidly frozen in liquid nitrogen until use at the synchrotron.

Protein Film Electrochemistry. Experiments were carried out in an anaerobic glovebox (MBraun) comprising a N_2 atmosphere ($O_2 < 2$ ppm). Buffers consisting of 0.05 M phosphate with 0.1 M NaCl as additional supporting electrolyte were prepared by using standard reagents NaCl, NaH_2PO_4, and Na_2HPO_4 (analytical reagent grade, Sigma). A pyrolytic graphite edge (PGE) rotating disk electrode (RDE, area 0.03 cm^2) was used in conjunction with an electrode rotator (EcoChemie). The all-glass electrochemical cell featured a Pt counter electrode placed in the main compartment and a saturated calomel electrode (SCE) as reference in a Luggin side arm. In this article, all potential values *E* have been adjusted to the standard hydrogen electrode (SHE) scale by using the relationship $E_{SHE} = E_{SCE} + 242$ mV. The cell was blacked out with black electrical tape to avoid light-activated processes convoluting the results (7, 16) and thermostated by a water-jacket linked to a water-circulator. To prepare an enzyme film, the PGE electrode was first polished for 10 s with an aqueous slurry of α-alumina (1 μm, Buehler) and sonicated for 5 s in purified water, before 1.5 μL enzyme solution (containing 0.02–0.2 μg *Cr*HydA1, i.e., up to $\approx$2 μM, pH 8) was applied and removed after a few minutes.

Electrochemical experiments were performed by using an electrochemical analyzer (Autolab PGSTAT20) controlled by a computer operating GPES software (EcoChemie). Mass flow controllers (Smart-Trak Series 100, Sierra Instruments) were used to prepare precise gas mixtures (accurate to within 1%) and to impose constant gas flow rates into the electrochemical cell during experiments. Depending on the nature of the experiment and the rate of the reaction, changes of gas conditions were performed by (*i*) changing the gas

mixture reaching the cell headspace, or (*ii*) by a simultaneous change in gas mixture in the headspace and injection of an aliquot of solution equilibrated with that gas. Efficient mixing and gas-solution equilibration were achieved through rapid electrode rotation (3,000 rpm).

X-Ray Absorption Measurements. K_α-fluorescence-detected XAS spectra at the Fe K-edge were collected at T = 20 K using an energy-resolving 13-element Ge detector and a helium cryostat as previously described (28, 29) at beamline D2 of the EMBL outstation (at HASYLAB, DESY). Harmonic rejection was achieved by detuning of the Si (111) double-crystal monochromator to 50% of its peak intensity. Spectra were collected maximally for a scan range of 6,950–8,450 eV. Deadtime-corrected XAS spectra were averaged after energy calibration of each scan by using the peak at 7,112 eV in the 1st derivative of the absorption spectrum of an Fe-foil as an energy standard (estimated accuracy ± 0.1 eV) (28, 29). Data were then normalized, and extended EXAFS oscillations were extracted (39). The energy scale of EXAFS spectra was converted to the wavevector scale (*k*-scale) by using an E_0 value of 7,112 eV. Unfiltered k^3-weighted spectra were used for least-squares curve-fitting employing a multiple-scattering approach with the program EXCURV (40). Fourier transforms were calculated from k^3-weighted EXAFS data by using the program SimX (39) and employing $\cos^2$ windows ranging >10% at both ends of the *k*-range. From experimental K-edge spectra the preedge peak region was extracted by using the program Xanda (www.bit.ly/1V1zKe).

ACKNOWLEDGMENTS. We thank the beamline scientist Dr. W. Meyer Klaucke (EMBL at DESY) for excellent technical support. We acknowledge Professor Achim Trebst for his teachings and for ongoing insightful discussions that made this work possible. We dedicate this article to him on the occasion of his 80th birthday. This work was funded by the Deutsche Forschungsgemeinschaft Grants SFB480 (to T.H.) and SFB498-C8 (to M.H.), the ''Unicat'' Cluster of Excellence Berlin, the EU/Energy Network SolarH2 (FP7 contract 212508), and Biotechnology and Biological Sciences Research Council Grant BB/D52222X/1 (to F.A.A.). K.A.V. is a Royal Society Research Fellow.

1. Vignais PM, Billoud B (2007) Occurrence, classification, and biological function of hydrogenases: An overview. *Chem Rev* 107:4206–4272.
2. Cammack R, Frey M, Robson R (2001) in *Hydrogen As a Fuel: Learning from Nature* (Taylor and Francis, London).
3. Adams MWW (1990) The structure and mechanism of iron hydrogenases. *Biochim Biophys Acta* 1020:115–145.
4. Parkin A, Goldet G, Cavazza C, Fontecilla-Camps JC, Armstrong FA (2008) The difference a Se makes? Oxygen-tolerant hydrogen production by the [NiFeSe]-hydrogenase from *Desulfomicrobium baculatum*. *J Am Chem Soc* 130:13410–13416.
5. Vincent KA, Parkin A, Armstrong FA (2007) Investigating and exploiting the electrocatalytic properties of hydrogenases. *Chem Rev* 107:4366–4413.
6. Hambourger M, et al. (2008) [FeFe]-hydrogenase-catalyzed H_2 production in a photoelectrochemical biofuel cell. *J Am Chem Soc* 130:2015–2022.
7. Parkin A, Cavazza C, Fontecilla-Camps JC, Armstrong FA (2006) Electrochemical investigations of the interconversions between catalytic and inhibited states of the [FeFe]-hydrogenase from *Desulfovibrio desulfuricans*. *J Am Chem Soc* 128:16808–16815.
8. Ghirardi ML, Dubini A, Yu JP, Maness PC (2009) Photobiological hydrogen-producing systems. *Chem Soc Rev* 38:52–61.
9. Nicolet Y, Piras C, Legrand P, Hatchikian C, Fontecilla-Camps JC (1999) *Desulfovibrio desulfuricans* iron hydrogenase: The structure shows unusual coordination to an active site Fe binuclear center. *Structure* 7:13–23.
10. Tard C, et al. (2005) Synthesis of the H-cluster framework of iron-only hydrogenase. *Nature* 433:610–613.
11. Peters JW, Lanzilotta WN, Lemon BJ, Seefeldt LC (1998) X-ray crystal structure of the Fe-only hydrogenase (*Cp*I) from *Clostridium pasteurianum* to 1.8 angstrom resolution. *Science* 282:1853–1858.
12. Pandey AS, Harris TV, Giles LJ, Peters JW, Szilagyi RK (2008) Dithiomethylether as a ligand in the hydrogenase H-cluster. *J Am Chem Soc* 130:4533–4540.
13. Nicolet Y, De Lacey AL, Vernede X, Fernandez VM, Hatchikian EC, Fontecilla-Camps JC (2001) Crystallographic and FTIR spectroscopic evidence of changes in Fe coordination upon reduction of the active site of the Fe-only hydrogenase from *Desulfovibrio desulfuricans*. *J Am Chem Soc* 123:1596–1601.
14. Silakov A, Reijerse EJ, Albracht SPJ, Hatchikian EC, Lubitz W (2007) The electronic structure of the H-cluster in the [FeFe]-hydrogenase from *Desulfovibrio desulfuricans*: A Q-band Fe-57-ENDOR and HYSCORE study. *J Am Chem Soc* 129:11447–11458.
15. Lubitz W, Reijerse E, van Gastel M (2007) [NiFe] and [FeFe] hydrogenases studied by advanced magnetic resonance techniques. *Chem Rev* 107:4331–4365.
16. Roseboom W, Lacey AL, Fernandez VM, Hatchikian EC, Albracht SPJ (2006) The active site of the [FeFe]-hydrogenase from *Desulfovibrio desulfuricans*. II. Redox properties, light sensitivity, and CO-ligand exchange as observed by infrared spectroscopy. *J Biol* Inorg Chem 11:102–118.
17. Lemon BJ, Peters JW (1999) Binding of exogenously added carbon monoxide at the active site of the iron-only hydrogenase (*Cp*I) from *Clostridium pasteurianum*. *Biochemistry* 38:12969–12973.
18. De Lacey AL, Stadler C, Cavazza C, Hatchikian C, Fernandez VM (2000) FTIR characterization of the active site of the Fe-hydrogenase from *Desulfovibrio desulfuricans*. *J Am Chem Soc* 122:11232–11233.
19. Cotton FA (1988) in *Advanced Inorganic Chemistry*, ed Cotton FA (Wiley, New York), p 58.
20. Kubas GJ (2007) Fundamentals of H_2 binding and reactivity on transition metals underlying hydrogenase function and H_2 production and storage. *Chem Rev* 107:4152–4205.
21. Erbes DL, King D, Gibbs M (1979) Inactivation of hydrogenase in cell-free-extracts and whole cells of *Chlamodomonas reinhardtii* by oxygen. *Plant Physiol* 63:1138–1142.
22. Crack JC, Green J, Cheesman MR, Le Brun NE, Thomson AJ (2007) Superoxide-mediated amplification of the oxygen-induced switch from [4Fe-4S] to [2Fe-2S] clusters in the transcriptional regulator FNR. *Proc Natl Acad Sci USA* 104:2092–2097.
23. Imlay JA (2006) Iron-sulphur clusters and the problem with oxygen. *Mol Microbiol* 59:1073–1082.
24. Kamp C, Silakov A, Winkler M, Reijerse EJ, Lubitz W, Happe T (2008) Isolation and first EPR characterization of the [FeFe]-hydrogenases from green algae. *Biochim Biophys Acta* 1777:410–416.
25. Stripp S, Sanganas O, Happe T, Haumann M (2009) The structure of the active site H-cluster of [FeFe] hydrogenase from the green alga *Chlamydomonas reinhardtii* studied by X-ray absorption spectroscopy. *Biochemistry* 48:5042–5049.
26. Winkler M, Heil B, Heil B, Happe T (2002) Isolation and molecular characterization of the [Fe]-hydrogenase from the unicellular green alga. *Chlorella fusca Biochim Biophys Acta* 1576:330–334.
27. Baffert C, et al. (2008) Hydrogen-activating enzymes: Activity does not correlate with oxygen sensitivity. *Angew Chem-Int* Ed 47:2052–2054.
28. Buhrke T, et al. (2005) Reduction of unusual iron-sulfur clusters in the H_2-sensing regulatory Ni-Fe hydrogenase from *Ralstonia eutropha* H16. *J Biol Chem* 280:19488–19495.
29. Loescher S, Schwartz L, Stein M, Ott S, Haumann M (2007) Facilitated hydride binding in an Fe-Fe hydrogenase active-site biomimic revealed by X-ray absorption spectroscopy and DFT calculations. *Inorg Chem* 46:11094–11105.
30. Goldet G, et al. (2009) Dynamic electrochemical investigations of hydrogen oxidation and production by enzymes and implications for future technology. *Chem Soc Rev* 38:36–51.
31. Fontecilla-Camps JC, Volbeda A, Cavazza C, Nicolet Y (2007) Structure/function relationships of [NiFe]- and [FeFe]-hydrogenases. *Chem Rev* 107:4273–4303.
32. Messner KR, Imlay JA (2002) Mechanism of superoxide and hydrogen peroxide formation by fumarate reductase, succinate dehydrogenase, and aspartate oxidase. *J Biol Chem* 277:42563–42571.
33. Varghese S, Tang Y, Imlay JA (2003) Contrasting sensitivities of *Escherichia coli* aconitases A and B to oxidation and iron depletion. *J Bacteriol* 185:221–230.
34. Tilley GJ, Camba R, Burgess BK, Armstrong FA (2001) Influence of electrochemical properties in determining the sensitivity of [4Fe-4S] clusters in proteins to oxidative damage. *Biochem J* 360:717–726.
35. Camba R, Armstrong FA (2000) Investigations of the oxidative disassembly of Fe-S clusters in *Clostridium pasteurianum* 8Fe ferredoxin using pulsed-protein-film voltammetry. *Biochemistry* 39:10587–10598.
36. Crack JC, Le Brun NE, Thomson AJ, Green J, Jervis AJ (2008) in *Globins and Other Nitric Oxide-Reactive Proteins, Part B* (Elsevier, San Diego, CA), pp 191–209.
37. Goldet G, et al. (2008) Hydrogen production under aerobic conditions by membrane-bound hydrogenases from *Ralstonia* species. *J Am Chem Soc* 130:11106–11113.
38. von Abendroth G, et al. (2008) Optimized over-expression of [FeFe] hydrogenases with high specific activity in *Clostridium acetobutylicum*. *Int J Hyd En* 33:6076–6081.
39. Dau H, Liebisch P, Haumann M (2003) X-ray absorption spectroscopy to analyze nuclear geometry and electronic structure of biological metal centers - Potential and questions examined with special focus on the tetra-nuclear manganese complex of oxygenic photosynthesis. *Anal Bioanal Chem* 376:562–583.
40. Tomic S, et al. (2004) New Tools for the Analysis of EXAFS: The DL-EXCURV Package. *CCLRC Technical Report* 1–10.